Complete solution of the two-dimensional antiferromagnetic Heisenberg model on small lattices

K. Fabricius, U. Löw, and K.-H. Mütter
Department of Physics, University of Wuppertal, D-5600 Wuppertal 1, Germany
(Received 29 April 1991)

We present the results of a complete and exact diagonalization of the antiferromagnetic Heisenberg Hamiltonian on 3×3, 3×4, 3×5, and 4×4 lattices with periodic boundary conditions.

I. INTRODUCTION

One of the oldest models for the description of antiferromagnetic ordering is the spin-$\frac{1}{2}$ quantum Heisenberg model. The interest in the thermodynamical and magnetic properties of this model goes back to the early times of quantum mechanics[1,2] and quantum chemistry[3] and experienced a renaissance when antiferromagnetic ordering[4] in two-dimensional planes had been observed in La_2CuO_4—one of the new high-T_c superconductors.[5]

Exact computations of the ground state of the antiferromagnetic Heisenberg (AFH) model were performed by Oitmaa and Betts[6] and extended to larger systems by Dagotto and Moreo.[7] Employing Monte Carlo techniques, Barnes and Swanson[8] estimated the low-lying energy eigenvalues on systems up to 64 sites. Variational techniques[9] were developed and refined to guess the ground-state wave function and the behavior of spin-spin correlation functions on large systems up to 256×256. The finite-temperature properties have been studied by several groups[10–12] performing Monte Carlo simulations on lattices up to 128×128. The results of Ref. 12 indicated that the correlation length diverges exponentially for $T\to0$, in accordance with the "classical" picture of Ref. 13.

Complete and exact diagonalizations of the AFH Hamiltonian have not yet been done for two-dimensional systems. For one-dimensional rings they were performed by Bonner and Fisher[14] and recently by the authors.[15]

It is the purpose of this paper to present the results of a complete and exact diagonalization of the AFH Hamiltonian on lattices:

$$3\times3,\quad 3\times4,\quad 3\times5,\quad 4\times4\ .$$

There are several reasons in favor of an exact solution of the eigenvalue problem on rather small systems.

(1) Nontrivial degeneracies of the eigenvalues may help to find "higher" conservation laws in the AFH model. In one dimension they are known to exist,[16,17]. In two dimensions nothing is known about them.

(2) The knowledge of the exact ground state $|0\rangle$ provides us with a sensitive measure (namely, the overlap $\langle0|\psi\rangle$) for the quality of any variational ansatz $|\psi\rangle$.

(3) Detailed structures, which cannot be resolved in a Monte Carlo simulation because of the inherent statistical errors, become visible in an exact calculation.

(4) There exist observables which are not accessible in a Monte Carlo simulation. Nevertheless they may contain important information on the properties of the model. In our study of the AFH model on rings,[15] the modulus of the momentum turned out to be such an observable. Its thermal average has the surprising property of being independent of the temperature.

The outline of this paper is as follows: In Sec. II the distributions and degeneracies of the energy eigenvalues are analyzed. In Sec. III a momentum analysis of the low-lying states is given together with the thermal averages of some momentum-dependent observables. They show the temperature independence found already on the rings. In Secs. IV and V the thermodynamical and magnetic properties are presented and compared with the Monte Carlo results of Ref. 12. The exact computation of the specific heat on a 4×4 lattice reveals a shoulderlike structure around $T=0.2$. Finally, in Sec. VI we check the quality of resonating-valence-bond- (RVB-) type trial functions[9] for the ground state by computing their overlap with the exact ground state.

II. ENERGY EIGENVALUES: NONTRIVIAL DEGENERACIES AND HIGHER SYMMETRIES

The two-dimensional isotropic antiferromagnetic Heisenberg model with periodic boundary conditions on a $L\times L$ lattice,

$$H=\sum_{\langle x,y\rangle}\mathbf{S}(x)\cdot\mathbf{S}(y)\ , \tag{2.1}$$

is symmetric under translations, rotations, and reflections. Therefore, the eigenvalues

$$\begin{aligned}&p_j=2\pi n_j/L,\quad j=1,2,\quad n_j=0,1,\ldots,L-1\ ;\\ &s=0,1,\ldots,L^2/2\ \text{ for } L^2 \text{ even}\ ;\\ &s=\tfrac{1}{2},\ldots,L^2/2\ \text{ for } L^2 \text{ odd}\ ;\\ &s_3=-s,\ldots,s\ ,\end{aligned} \tag{2.2}$$

of the momentum operators P_j, $j=1,2$ and total-spin operators $\mathbf{S}^2,S_3$ are "good" quantum numbers for the characterization of the energy eigenstates:

$$|E,s,s_3,p_1,p_2\rangle\ . \tag{2.3}$$

States with momenta $\mathbf{p}=(0,0),(\pi,\pi)$ can be further classified according to their transformation properties under rotations:

$$|E,s,s_3,\mathbf{p}=(0,0),(\pi,\pi),m\rangle \ . \tag{2.4}$$

The quantum number m for the angular momentum takes the values

$$m=-1,0,1,2 \ . \tag{2.5}$$

Under reflections, states with angular momentum m are transformed into those with angular momentum $-m$ (where $m=-2$ is identical to $m=2$).

There are trivial degeneracies of the energy eigenstates with (i) different values of s_3 and s fixed, (ii) "equivalent" values of $\mathbf{p}$, which are related by rotations and reflections on the (two-dimensional) lattice, and (iii) momentum (0,0) or (π,π) and angular momenta $m=-1,1$. Any further degeneracy of energy eigenvalues is a hint to the existence of higher conservation laws. An example of nontrivial degeneracies is given in Table I, where we list the lowest eigenstates of the AFH Hamiltonian on a 4×4 lattice.

TABLE I. Quantum numbers of the low-lying states on a 4×4 lattice: energy per spin, total spin, and "inequivalent" momenta. Note that some of the momentum vecotrs (0,0),(2,2) occur twice (last column). These degenerate states differ in their angular momentum $m=-1,1$.

Energy	Spin	Momenta		
$-7.017\,802\,005\,268\,03\times10^{-1}$	0	00		
$-6.656\,178\,045\,414\,66\times10^{-1}$	1	22		
$-5.948\,554\,989\,960\,78\times10^{-1}$	2	00		
$-5.554\,026\,504\,879\,06\times10^{-1}$	1	12		
$-5.496\,486\,817\,585\,94\times10^{-1}$	1	01		
$-5.323\,927\,247\,648\,78\times10^{-1}$	1	20	11	
$-5.158\,016\,848\,317\,45\times10^{-1}$	0	00	02	
$-4.923\,690\,869\,607\,52\times10^{-1}$	0	12	10	
$-4.897\,835\,983\,424\,89\times10^{-1}$	3	22		
$-4.882\,592\,505\,595\,16\times10^{-1}$	0	11	22	22
$-4.853\,546\,409\,792\,30\times10^{-1}$	2	01		
$-4.804\,521\,453\,778\,93\times10^{-1}$	0	00		
$-4.768\,883\,226\,619\,51\times10^{-1}$	2	21		
$-4.673\,158\,313\,872\,00\times10^{-1}$	2	11	20	
$-4.645\,378\,378\,786\,03\times10^{-1}$	1	11	00	00
$-4.618\,723\,862\,262\,69\times10^{-1}$	1	12	01	
$-4.608\,998\,651\,801\,91\times10^{-1}$	1	22	20	
$-4.455\,327\,109\,130\,06\times10^{-1}$	0	11	20	
$-4.359\,252\,305\,289\,88\times10^{-1}$	0	12		
$-4.319\,269\,336\,727\,91\times10^{-1}$	0	10		
$-4.235\,480\,936\,333\,84\times10^{-1}$	2	00	02	
$-4.224\,754\,237\,457\,31\times10^{-1}$	0	02	00	
$-4.209\,606\,319\,967\,88\times10^{-1}$	1	02	11	
$-4.169\,662\,418\,600\,47\times10^{-1}$	1	11	20	
$-4.161\,937\,842\,173\,03\times10^{-1}$	1	01		
$-4.145\,562\,285\,776\,56\times10^{-1}$	1	22		
$-4.117\,309\,332\,175\,66\times10^{-1}$	1	21		
$-4.115\,406\,192\,901\,59\times10^{-1}$	0	10	12	
$-4.072\,034\,892\,611\,81\times10^{-1}$	0	11	22	22
$-4.059\,984\,921\,488\,66\times10^{-1}$	2	11	02	
$-4.033\,064\,755\,665\,25\times10^{-1}$	2	20	22	
$-4.029\,613\,531\,242\,59\times10^{-1}$	0	12		
$-3.991\,660\,003\,711\,03\times10^{-1}$	1	12	01	
$-3.982\,015\,332\,061\,19\times10^{-1}$	2	11	22	22
$-3.931\,766\,662\,348\,56\times10^{-1}$	1	12		
$-3.919\,761\,018\,811\,47\times10^{-1}$	1	22	00	

tice.

There are four types of multiplets, characterized by a unique value of the total spin s, but different "inequivalent" values of the momenta:

$$\mathbf{p}=\frac{\pi}{2}\mathbf{n}, \quad \mathbf{n}=(0,0),(0,1),(0,2),(1,1),(1,2),(2,2) \ . \tag{2.6}$$

(1) "Doublet" states always have momenta

$$\mathbf{n}=(0,0),(2,2) \tag{2.7}$$

They appear in the total-spin sectors $s=0,1,2,3,4,5$.

(2) There are two types of "triplet" states with momenta:

$$\mathbf{n}=(0,0),(0,2),(2,0) \ , \tag{2.8}$$

$$\mathbf{n}=(2,2),(0,2),(2,0) \ . \tag{2.9}$$

They appear in the total-spin sectors $s=0,1,2,3,4,5,6$.

(3) There are three types of "sextet" states:

$$\mathbf{n}=(1,1),(-1,-1),(-1,1),(1,-1),(0,2),(2,0) \ , \tag{2.10}$$

$$\mathbf{n}=(1,1),(-1,-1),(-1,1),(1,-1),(2,2),(2,2) \ , \tag{2.11}$$

$$\mathbf{n}=(1,1),(-1,-1),(-1,1),(1,-1),(0,0),(0,0) \ . \tag{2.12}$$

(4) "Octet" states always have momenta

$$\mathbf{n}=(0,1),(0,-1),(1,0),(-1,0),(1,2),(-1,2),(2,1),(2,-1) \ . \tag{2.13}$$

Octets appear in the total-spin sectors $s=0,1,2,3,4,5,6$.

The underlying symmetry of this multiplet structure has a simple geometric origin. The 4×4 lattice with periodic boundary conditions can be mapped onto the four-dimensional hypercube 2^4 (again with periodic boundary conditions) in such a way that nearest-neighbor couplings correspond to nearest-neighbor couplings. Therefore, in this special case it is more appropriate to classify the energy eigenstates according to the four-momenta $p=\pi(n_1,n_2,n_3,n_4)$, $n_j=0,1$, on the hypercube. Note that there are only five inequivalent four-momenta. The eigenstates with four-momenta $p=(0,0,0,0)$ and $p=\pi(1,1,1,1)$ can be further classified according to the irreducible representations of the four-dimensional rotations on the hypercube. In particular, the ground state as a four-momentum 0 state is invariant under these rotations.

In Figs. 1(a)–1(f) the distributions $N(E,s)$ of the energy eigenvalues in the total-spin sectors are shown for two AFH Hamiltonians: (a) on a 4×4 lattice (solid line) and (b) on a ring with 16 sites (dashed line). We observe that the distributions on the two-dimensional system are narrower than on the ring. On both systems the small energy eigenvalues are accompanied by small eigenvalues of the total spin s.

III. THERMAL AVERAGE OF THE MOMENTUM

In Figs. 2(a)–2(f) the distributions of the energy eigenvalues in the six momentum sectors listed in Eqs. (2.6) are plotted. They look almost the same, independent of the momentum vector $\mathbf{p}$. A similar feature had been ob-

served already on the ring with $L=16$ sites.[15]. In that case we suggested the distributions $N(E,p=2\pi n/L)$ to be momentum independent in the thermodynamical limit $L\to\infty$. Such a hypothesis fixes the thermal average of the modulus of the momentum:

$$\langle |p| \rangle(T)=\pi/2 \quad \text{for } T>0 \ . \tag{3.1}$$

On the ring with $L=16$, this behavior is clearly seen for $T>0.5$.

In two dimensions the momentum independence of the distributions $N(E,\mathbf{p})$ leads to the predictions

$$\langle |p_j| \rangle(T)/c_j=1 \quad \text{for } j=1,2 \ , \tag{3.2}$$

$$\langle (p_1^2+p_2^2)^{1/2} \rangle(T)/c=1 \ . \tag{3.3}$$

The values of the constants c_j and c on the lattices,

$$3\times3, 3\times4, 3\times5, 4\times4 \ , \tag{3.4}$$

are given in Table II. In Figs. 3(a) and 3(b) we have plotted the left-hand sides of equations (3.2) and (3.3). For $T>1$ we find what is expected from the momentum independence of the distributions $N(E,\mathbf{p})$. For smaller values of T, however, there are strong deviations. They have their origin in the momenta of the low-lying states on the finite systems (3.4), which can be read off Table II.

Just as in the one-dimensional case,[15] we expect the deviations from the constant behavior (3.2) and (3.3) to be mere finite-size effects. This would imply that (3.2) and (3.3) are correct for all temperatures in the thermodynamical limit.

IV. INTERNAL ENERGY, ENTROPY, AND SPECIFIC HEAT

From the distribution of energy eigenvalues, we compute the thermodynamical properties of the AFH model. In Figs. 4 and 5 the internal energy per site and specific heat are shown for the lattices (3.4). The specific heat shows two characteristic features.

(1) There is a maximum around $T=0.6$. Its position is rather independent of the lattice size, whereas its width seems to shrink with increasing lattice size.

(2) At small temperatures $T=0.2$, a shoulder appears for the largest lattice 4×4. Note that such a structure is

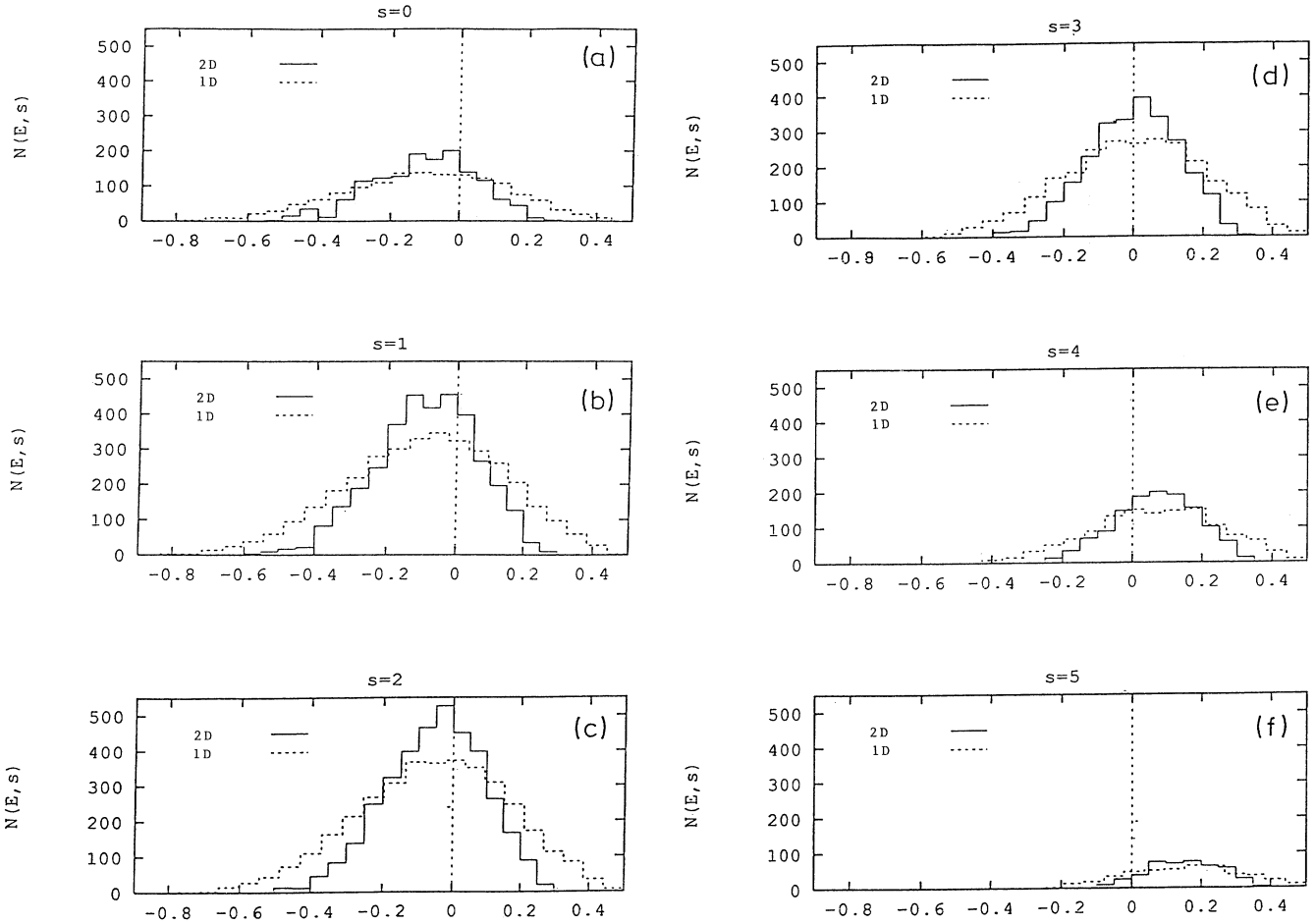

FIG. 1. Densities of states $N(E,s)$ in the sectors with total spin $s=0,1,2,3,4,5$ on a 4×4 lattice.

TABLE II. Energy per site $(\varepsilon_0,\varepsilon_1)$, total spin (s_0,s_1), momentum $(\mathbf{p}_0,\mathbf{p}_1)$, and the degeneracy (d_0,d_1) of the ground and first excited states. The coefficients c_1,c_2,c appearing in Eqs. (3.2) and (3.3) are listed in the last three rows.

Lattice	3×3	3×4	3×5	4×4
$-\varepsilon_0$	0.441 000 194 4	0.614 018 14	0.528 456 52	0.701 780 2
s_0	$\frac{1}{2}$	0	$\frac{1}{2}$	0
$\mathbf{p}_0/2\pi$	$(\frac{1}{3},\frac{2}{3})$	(0,0)	$(\frac{2}{3},\frac{4}{5})$	(0,0)
d_0	8	1	8	1
$-\varepsilon_1$	0.409 571 184	0.539 710 979	0.506 487 214 7	0.665 617 8
s_1	$\frac{1}{2}$	1	$\frac{1}{2}$	1
$\mathbf{p}_1/2\pi$	$(\frac{1}{3},0)$	$(\frac{1}{3},\frac{1}{2})$	$(0,\frac{4}{5})$	$(\frac{1}{2},\frac{1}{2})$
d_1	8	6	4	3
c_1/π	$\frac{4}{9}$	$\frac{4}{9}$	$\frac{4}{9}$	$\frac{1}{2}$
c_2/π	$\frac{4}{9}$	$\frac{1}{2}$	$\frac{12}{25}$	$\frac{1}{2}$
c/π	0.7945	0.7558	0.7339	0.7153

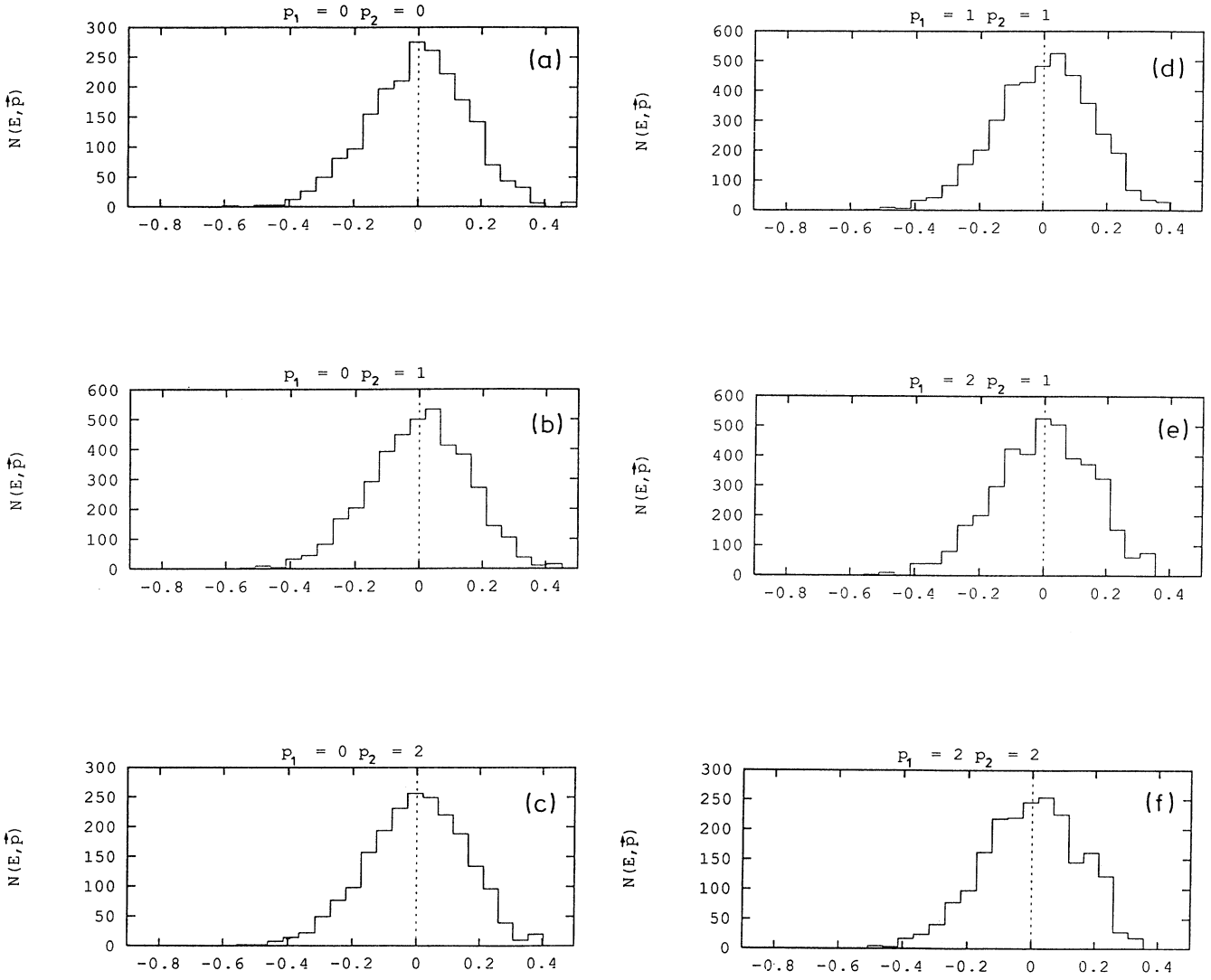

FIG. 2. Densities of states $N(E,\mathbf{p})$ for the inequivalent momenta (2.6)

absent on the smaller lattices 3×3, 3×4, and 3×5. Therefore, it is rather implausible to interpret this shoulder as a mere finite-size effect.

Figures 4 and 5 also contain the results of Table I in Ref. 12, which were obtained by a quantum Monte Carlo study on rather large square lattices $L\times L$, with L ranging from 24 to 128. The internal energy on these large lattices is bounded from below and above by our results on the 4×4 and 3×4 lattice, respectively. This reminds us of the one-dimensional case,[15] where the internal energy per site in the thermodynamical limit $L\to\infty$ is bounded from above and below by the corresponding quantity on a finite ring with L odd and even, respectively. In order to estimate the behavior in the thermodynamical limit, we proceed here in the same way as we did in the one-dimensional case. We start with an ansatz:

$$u(T)=p_1u_1(T)+p_2u_2(T)\ , \tag{4.1}$$

where $u_1(T)$ and $u_2(T)$ are the internal energies per site on the lattices 4×4 and 3×4, respectively. The weights p_1 and p_2 are assumed to be temperature independent. Their values are fixed by the ground-state energy:

$$u(T=0)=0.668\ . \tag{4.2}$$

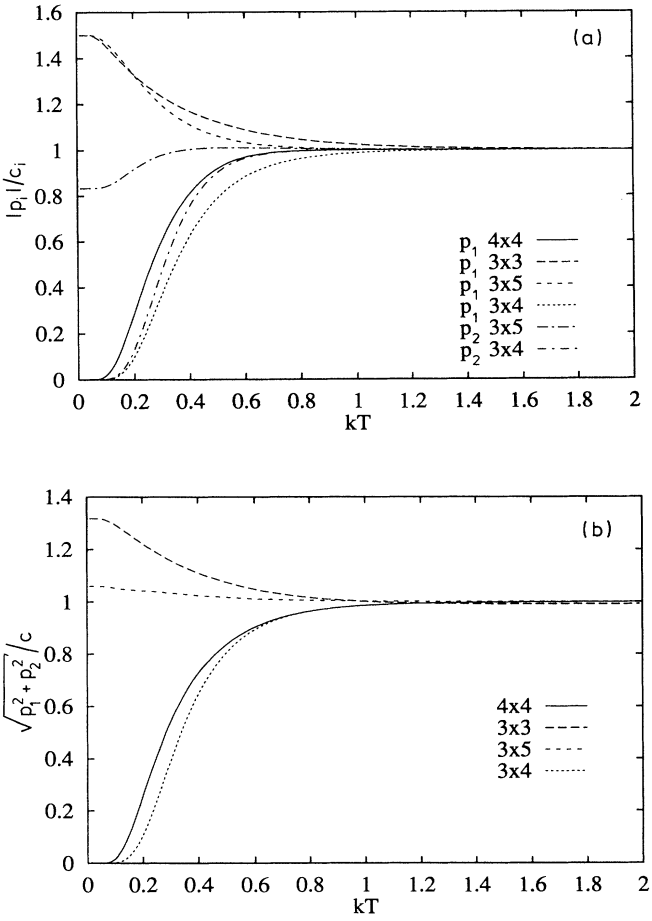

FIG. 3. Thermal averages $\langle|p_j|\rangle(T)/c_j$ and $\langle(p_1^2+p_2^2)^{1/2}\rangle(T)/c$ as a function of the temperature.

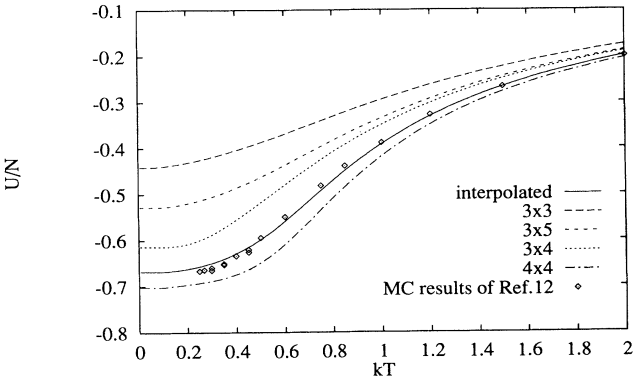

FIG. 4. Internal energy per site on the lattices (3.4) together with the Monte Carlo results of Ref. 12 and the interpolation (4.1).

This is so far the best estimate, obtained by Huser and Elser[9] on the basis of a variational calculation. From this value we get the weights

$$p_1=0.614,\quad p_2=0.386\ . \tag{4.3}$$

The interpolation (4.1) is represented by the solid curve in Fig. 4. The Monte Carlo data of Ref. 12 are very close to this curve.

Concerning the specific heat, the Monte Carlo data lie just in between our results on the 4×4 and 3×4 lattices, except for the points at $T=0.45$ and 0.5, which are close to the point where the 4×4 and 3×4 curves cross each other.

The interpolation of the specific heats $c_1(T)$ and $c_2(T)$ on the lattices 4×4 and 3×4,

$$c(T)=p_1c_1(T)+p_2c_2(T)\ , \tag{4.4}$$

yields a fairly good description of the Monte Carlo data. It is remarkable that the maximum in the specific heat is higher and narrower on the 4×4 lattice than in the Monte Carlo data on much larger systems.

At this point we would like to stress that detailed structures at low temperatures (such as the shoulder at

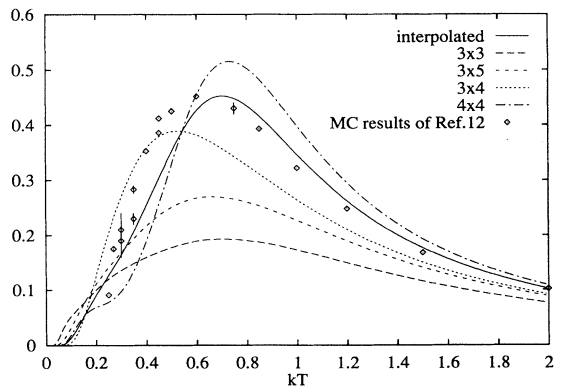

FIG. 5. Specific heat on the lattices (3.4) together with the Monte Carlo results of Ref. 12 and the interpolation (4.4)

$T=0.2$) can be resolved in an exact computation only. If such structures survive in the thermodynamical limit, it will be extremely hard to extract the low-temperature behavior from a Monte Carlo simulation in a reliable way.

In Fig. 6 the entropy per site versus temperature is plotted. The finite zero-temperature entropy on the lattices 3×3 and 3×5 reflects the degeneracy of the ground state in these systems (cf. Table II). Note also the change in slope at $T=0.4$ on the 4×4 lattice. This is close to the temperature where the specific heat has the shoulder mentioned above.

V. UNIFORM SUSCEPTIBILITY AND STAGGERED MAGNETIZATION

The uniform susceptibility $\chi(T)$ is related to the thermal average $\langle \mathbf{S}^2 \rangle(T)$ of the square of the total spin:

$$\mathbf{S}=\sum_x \mathbf{S}(x) , \tag{5.1}$$

$$\chi(T)=(3NkT)^{-1}\langle \mathbf{S}^2 \rangle . \tag{5.2}$$

Figure 7 shows the thermal averages of $\mathbf{S}^2$ on the lattices (3.4) as a function of the temperature. The different low-temperature behavior of this quantity on systems with an even and an odd number N of sites is a reflection of the different spin values for the low-lying states (cf. Table II). Just as we observed in the entropy, there is a slight change in the slope of this quantity on the 4×4 lattice around $T=0.4$.

The uniform susceptibility on the lattices 4×4 and 3×4 is shown in Fig. 8 together with an interpolation (solid line),

$$\chi(T)=p_1\chi_1(T)+p_2\chi_2(T) , \tag{5.3}$$

with weights (4.3). It fits nicely the Monte Carlo data of Ref. 12, except for the lowest-temperature values.

Let us now turn to the thermal average $L^{-4}\langle \mathbf{S}_{\rm st}^2 \rangle$ of the square of the staggered spin:

$$\mathbf{S}_{\rm st}=\sum_x (-1)^x \mathbf{S}(x) . \tag{5.4}$$

In the thermodynamical limit $L\to\infty$, it is related to the staggered magnetization

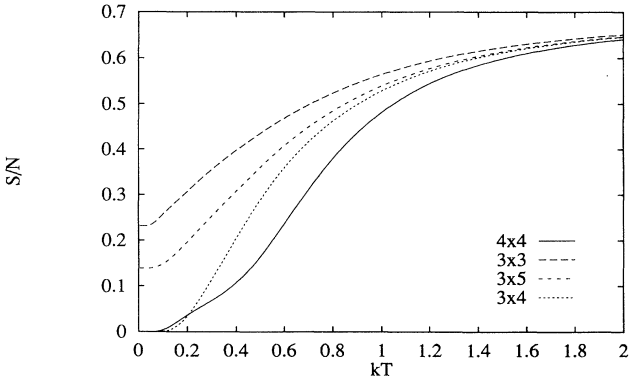

FIG. 6. Entropy per site on the lattices (3.4).

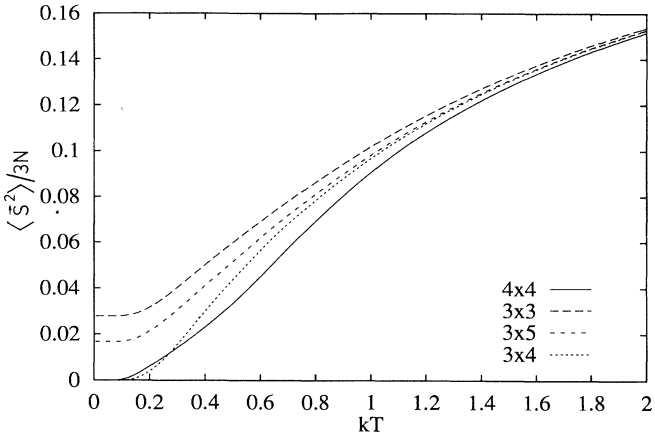

FIG. 7. Thermal average of $\mathbf{S}^2$ on the lattices (3.4).

$$m^+=\lim_{L\to\infty} L^{-2}\langle \mathbf{S}_{\rm st}^2 \rangle^{1/2} . \tag{5.5}$$

This quantity was calculated for $T=0$ on a 4×4 lattice by Oitmaa and Betts[6] and on a 6×4 lattice by Dagotto and Moreo:[7]

$$16^{-2}\langle \mathbf{S}_{\rm st}^2 \rangle(T=0)=0.276 , \tag{5.6}$$

$$24^{-2}\langle \mathbf{S}_{\rm st}^2 \rangle(T=0)=0.2341 . \tag{5.7}$$

Series expansions performed by Huse[18] and the Monte Carlo simulations of Reger and Young[19] lead to the following estimate for this quantity in the thermodynamical limit:

$$(m^+)^2=0.09 . \tag{5.8}$$

Therefore, finite-size effects for this quantity are enormous and puzzling.

Figure 9 shows our result for $16^{-2}\langle \mathbf{S}_{\rm st}^2 \rangle(T)$ as a function of T. At $T=0$ we agree with the value (5.6) of Ref. 6. We have also included the Monte Carlo data of Ref. 12. It is interesting to see that the extrapolation of the

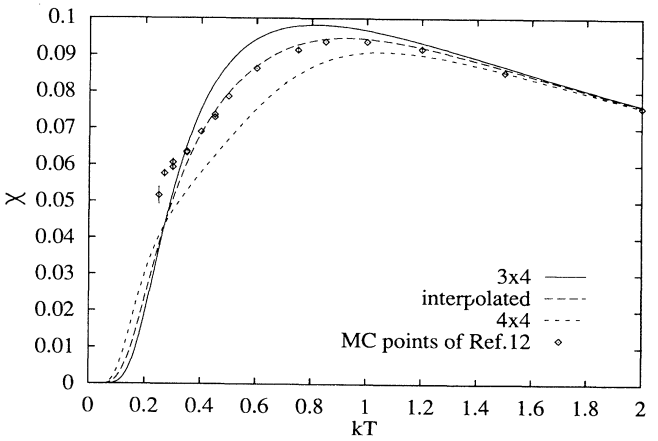

FIG. 8. Uniform susceptibility on the 4×4 lattice together with the Monte Carlo results of Ref. 12 and the interpolation (5.3).

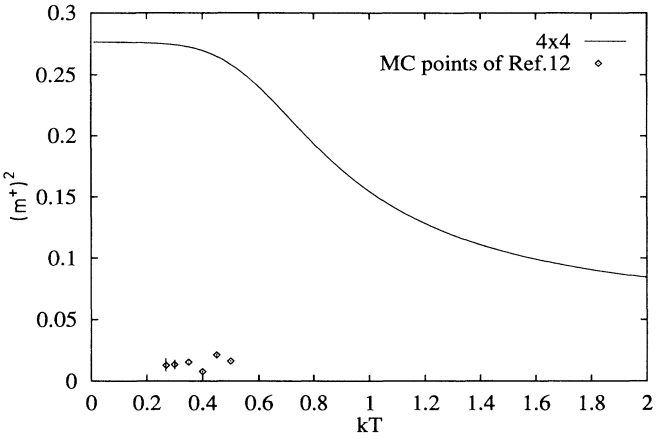

FIG. 9. Staggered magnetization squared the 4×4 lattice together with the Monte Carlo results of Ref. 12.

Monte Carlo data from $T=0.3$ to 0 has to increase by a factor of 8 in order to meet the value (5.8) of Refs. 18 and 19.

VI. STRUCTURE OF THE GROUND STATE

There have been many attempts made to guess the ground state $|0\rangle$ of the two-dimensional AFH model in the thermodynamical limit. For an even number of sites, the ground state has total spin 0. Therefore, one usually starts with a superposition of valence-bond states $|K\rangle$:

$$|0\rangle=\sum_K c(K)|K\rangle \ . \tag{6.1}$$

The sum extends over all valence-bond configurations K. They are obtained by connecting pairs of sites x,y by a straight line. The spins at the paired sites x and y are coupled to zero:

$$[x,y]=2^{-1/2}[\chi_+(x)\chi_-(y)-\chi_-(x)\chi_+(y)] \ . \tag{6.2}$$

The valence-bond state $|K\rangle$ is defined as the product wave function for all pairs on K:

$$|K\rangle=\prod_j [x_j,y_j] \ . \tag{6.3}$$

The valence-bond states form an overcomplete nonorthogonal basis. Some of the linear dependences can be easily eliminated. For example, valence-bond states (6.3) with spin-0 couplings only among even and odd sites $x\epsilon S_+$ and $y\epsilon S_-$ form a complete set as well. In the following we will consider trial functions (6.1), which are superpositions of such states.

Various choices have been proposed for the coefficients $c(K)$ in the expansion (6.1). For example, in Ref. 9 a factorizing ansatz with weights $h(|x-y|)$ depending on the bond length is made:

$$c(K)=\prod_j h(|x_j-y_j|) \ . \tag{6.4}$$

This ansatz is a generalization of the RVB state with nearest-neighbor coupling ("dimer") only. The best choice of the weight function $h(|x-y|)$ has been found by the authors of Ref. 9 by minimizing the ground-state energy.

Here we want to propose an alternative to the ansatz (6.4):

$$c(K)=f(N_d(K)) \ . \tag{6.5}$$

The weights only depend on the number of dimers $N_d(K)$ on each configuration K. Therefore, the variational ansatz operates in the $(V/2+1)$-dimensional subspace spanned by the states $|j\rangle$ with fixed dimer number $j=N_d(K)=0,1,2,\ldots V/2$. V is the number of sites:

$$|j\rangle=\sum_K \delta_{j,N_d(K)}|K\rangle \ . \tag{6.6}$$

The variational parameters $f(j)$ are fixed by diagonalizing the AFH Hamiltonian in this subspace.

In Table III we list energy expectation values per spin and the overlap with the exact ground state for four types of wave functions on a 4×4 lattice: (i) the Néel state $|1\rangle$; (ii) the RVB state with dimers, $|2\rangle$; (iii) the RVB state with variational parameters depending on the bond length [$h(1)/h(3)=0.278$; cf. P.W. Anderson *et al.* in Ref. 9], $|3\rangle$; and (iv) the RVB state with optimized variational parameters depending on the dimer number, $|4\rangle$.

TABLE III. Energy per spin and overlap with the exact ground state on a 4×4 lattice for the trial states $|j\rangle$, $j=1,2,3,4$, defined in the text.

State	$\|1\rangle$	$\|2\rangle$	$\|3\rangle$	$\|4\rangle$
$\varepsilon_j-\varepsilon_0$	0.201 78	0.047 227 5	1.03×10^{-4}	0.663×10^{-4}
$1-\langle 0\|j\rangle$	0.59	0.074 415 05	0.931×10^{-4}	0.504×10^{-4}

The results for the Néel state $|1\rangle$ and the RVB state with dimers, $|2\rangle$, have been obtained before by Dagotto and Moreo (cf. Table V in Ref. 7). We do not agree with their number for the overlap $\langle 0|2\rangle$.

VII. CONCLUSIONS

Exact and complete solutions of the eigenvalue problem for the AFH model are feasible only on small lattices. Nevertheless, they are needed for a quantitative check of approximations and other methods which suffer from inherent systematic and/or statistical errors. Moveover, they may reveal new features, as we found in our solution on a 4×4 lattice.

(1) The distributions $N(E;\mathbf{p})$ appear to be momentum independent. As a consequence, the thermal averages of the momentum-dependent observables (3.2) and (3.3) are temperature independent.

(2) The specific heat on the 4×4 lattice develops a peak around $T=0.7$, which is more pronounced in height and width than the peak in the Monte Carlo data of Ref. 12 obtained on large lattices $L\times L$ ($24<L<128$).

(3) At low temperatures ($T=0.2$) a shoulderlike structure is visible in the specific heat on the 4×4 lattice.

(4) The energy eigenstates show nontrivial degeneracies which can be understood by mapping the 4×4 lattice

onto the "more symmetric" 2^4 hypercube. This mapping is a special example for the fact that the two-dimensional AFH Hamiltonian on a finite lattice may be invariant under "nontrivial" permutations of the sites, which are not associated with translations, rotations, and reflections. Another example for a planar system with ten sites has been given by Saito.[20]

We have demonstrated that the behavior of the internal energy, specific heat, and uniform susceptibility in the thermodynamical limit can be estimated by an interpolation of these quantities on rather small lattices. On the other hand, the staggered magnetization squared is an extremely size-dependent quantity, which needs further investigation.

Note added in proof. We were informed by E. Dagotto that the staggered magnetizations quoted in Ref. 7 are incorrect. The correct value on the 6×4 lattice is given in Eq. (5.7).

[1]H. A. Bethe, Z. Phys. **71**, 205 (1931).
[2]L. Hulthén, Ark. Mat. Astron. Fys. A **26** (11), 1 (1938).
[3]L. Pauling, J. Chem. Phys. **1**, 280 (1933).
[4]Y. Endoh *et al.*, Phys. Rev. B **37**, 7443 (1988); G. Aeppli *et al.*, Phys. Rev. Lett. **62**, 2052 (1989).
[5]J. G. Bednorz and K. A. Müller, Z. Phys. B **64**, 188 (1986); C. W. Chu *et al.*, Phys. Rev. Lett. **58**, 405 (1987).
[6]J. Oitmaa and D. D. Betts, Can. J. Phys. **56**, 897 (1978); J. Borysowicz, P. Horsch, and T. Kaplan; Phys. Rev. B **31**, 1590 (1985).
[7]E. Dagotto and A. Moreo, Phys. Rev. B **38**, 5087 (1989).
[8]T. Barnes and E. Swanson, Phys. Rev. B **37**, 9405 (1988).
[9]P. W. Anderson, B. Doucot, and S. Liang, Phys. Rev. Lett. **61**, 365 (1988); D. A. Huse and V. Elser, Phys. Rev. Lett. **60**, 2531 (1988); H. Yokoyama and H. Shiba, J. Phys. Soc. Jpn. **56**, 3570 (1987); C. Gros, R. Joyut, and T. M. Rice, Z. Phys. B **68**, 425 (1987).
[10]D. H. Lee, J. D. Joannopoulos, and J. W. Negele, Phys. Rev. B **30**, 1599 (1984); G. Gomez-Santoz, J. D. Joannopoulos, and J. W. Negele, *ibid.* **39**, 4435 (1989).
[11]E. Manousakis and R. Salvador, Phys. Rev. Lett. **60**, 840 (1988); Phys. Rev. B **39**, 575 (1987).
[12]Hong-Qiang Ding and Miloje S. Makivic, Phys. Rev. Lett. **64**, 1449 (1990); Phys. Rev. B **43**, 3562 (1991).
[13]S. Chakravarty, B. I. Halperin, and D. Nelson, Phys. Rev. Lett. **60**, 1057 (1988); Phys. Rev. B **39**, 2344 (1989).
[14]J. C. Bonner and M. E. Fisher, Phys. Rev. **135**, A640 (1964).
[15]K. Fabricius, U. Löw, K.-H. Mütter, and P. Ueberholz, Phys. Rev. B **44**, 7476 (1991).
[16]M. Lüscher, Nucl. Phys. **B117**, 475 (1976).
[17]K. Fabricius, K.-H. Mütter, and H. Grosse, Phys. Rev. B **42**, 4656 (1990).
[18]D. A. Huse, Phys. Rev. B **37**, 2380 (1988).
[19]J. D. Reger and A. P. Young, Phys. Rev. B **37**, 5978 (1988).
[20]R. Saito, Solid State Commun. **72**, 517 (1989).